STRESS CORROSION CRACKING IN DEPLETED URANIUM -2 W/O MOLYBDENUM ALLOY PENETRATORS

By C. R. Crowe*

D. F. Hasson**

H. A. Newborn*

J. A. Joyce**

* Naval Surface Weapons Center, Silver Spring, Maryland 20910

** U. S. Naval Academy, Annapolis, Maryland 21402

Abstract

High kinetic energy rounds are required for a variety of defense systems and dense uranium alloys are well suited for this application. A problem area involves storage of the rounds for extended periods in marine environments. Uranium is highly susceptible to general atmospheric corrosion and, more critically, to stress corrosion cracking (SCC). To date, coating schemes have achieved limited success in alleviating these problems. In general, alloying of uranium with elements such as molybdenum, tends to improve resistance to uniform corrosion but results in a multi-phased structure and high SCC susceptibility.

Stress corrosion cracking in alloys in salt laden, moist air environments has been studied by cantilever beam testing. Crack growth kinetics were continuously monitored during the test. Threshold stress intensity values for SCC, K_{1scc}, range from 24.4 MPa.$m^{1/2}$ to 15.6 MPa.$m^{1/2}$ for DU-3/4 Ti and DU-Quint, respectively. Values for U-2Mo in two heat treated conditions were slightly less than the DU-3/4 Ti threshold. Data are presented in a "safe zone" plot of flaw size vs. stress. Fractographic investigations by SEM revealed mixed fracture modes with both transgranular and intergranular fracture occurring.

The SCC failure mechanism is caused by the conjoint action of localized stress and a corrosive medium. Earlier work has shown that crack propagation is rapid in U-2Mo. Presently, rounds are produced by hot rolling and grinding of U-2Mo bar or rod stock. Stress corrosion cracking in penetrators fabricated in this way has been reported during long-term exposures to humid air. Cracking was linked to the presence of residual stresses and oxycarbonnitride inclusions in the material. These inclusions provide regions of stress concentration and localized corrosive attack which serve as sites for crack

initiation. Tensile stresses are necessary for crack propagation and these may result from corrosion product wedging and/or residual tensile stress produced during fabrication of the round. Since α-uranium is very anisotropic mechanically, some internal stress always remains locked into any polycrystalline part even after "stress relief" heat treatments.

Acknowledgments

The authors would like to extend their appreciation to Messrs. F. Rider, R. Jones, D. Eller, and Dr. M. Norr for technical assistance. Funding for this work was provided by Naval Sea Systems Command, and the Naval Surface Weapons Center under Independent Research Projects.

INTRODUCTION

A depleted uranium -2 weight percent molybdenum alloy (U-2Mo) has been selected as penetrator material for various defense systems. One problem with the use of U-2Mo, as well as other uranium based alloys, is that the alloy is susceptible to stress corrosion cracking (SCC) during storage in moist air environments, especially if sodium chloride is also present. Indeed, catastrophic SCC failure of penetrators during long-term exposure to humid air has been observed (Figure 1).

During the last five years, detailed studies of the stress corrosion cracking problem have been conducted at the Naval Surface Weapons Center (NSWC). These studies have linked the SCC phenomena with the presence of both residual stresses and oxycarbonitride inclusions in the material.[1,2] The inclusions provide regions of stress concentration and localized corrosive attack and serve as sites for crack initiation. Tensile stresses are necessary for SCC crack propagation. Tensile stresses in rounds result from corrosion product wedging and/or residual tensile stress produced during fabrication of the round. Internal stresses in parts produced from depleted uranium alloys result from the concomitant factors of plastic deformation, thermal strains, and phase transformations during fabrication. In other uranium alloy munitions the $\lambda \rightarrow \alpha'$ transformation is of such magnitude as to sometimes cause centerline void formation.[3]

Initial penetrators were fabricated at NL Industries, Albany, NY, by grinding hot rolled U-2Mo rod. Since this technique is time consuming, expensive, and wasteful of material, other production techniques have been examined. The feasibility of forging the rounds has been demonstrated by NETCO, Long Beach, CA., and casting techniques have been developed at Nuclear Metals, Inc., Concord, MA. Each of the manufacturing methods produce different internal stress states which must be assessed as to their effect on the stress corrosion cracking phenomena.

A correlation of the stress distributions with SCC crack propagation characteristics is presented.

Diagnostic tests were also performed on the rounds including hardness and yield strength measurements, moist nitrogen environmental tests, and microstructural determinations. In addition, detailed chemical analysis was performed on the rounds for comparison with inclusion content in the microstructure. Scanning electron microscopy was performed on SCC fracture surfaces.

The results of measurement of residual internal stress distributions occurring in rounds manufactured by these methods is described.

Although rounds using other DU alloys were not produced, SCC kinetics in U-3/4 Ti, and U-3/4 Quint alloys are also reported with those of U-2Mo in moist salt laden air using precracked cantilever beam specimens for comparison. The fracture mechanics approach for stress corrosion tests as suggested by Brown and Beachem[4] is used. This data is then utilized to construct the so called "safe-zone" plot for the use of the alloys in moist salt laden air.[5,6]

EXPERIMENTAL PROCEDURES

I. MATERIALS

Table 1 lists the representative samples from forged and cast batches tested, along with a description of post-working heat treatments. Chemical analysis of the rounds was performed by Ledoux and Co. with the results listed in Table 2.

Hardness measurements were made using both the Rockwell "C" and Knoop microhardness scales. The mean values are tabulated in Table 3 along with yield strength data for the various lots. Compressive stress-strain curves were measured using the cylindrical portion of the rounds for the tests.

A 0.2% offset yield stress determination was made, though inherent inaccuracy is recognized due to the low length to diameter ratio of 1.6:1 of the specimens and the anelastic behavior of uranium alloys.

A round from each batch was cut lengthwise, mounted, polished, and etched for metallographic examination. The etchant which produced the best results was one part each of nitric acid, acetic acid, and water, adding a few drops of hydrofluoric acid. Illustrative microstructures are shown in Figure 2.

All materials used in SCC testing were processed and fabricated into specimens by Rockwell International Corporation, Rocky Flats Division except for tensile and Charpy V-notch specimens which were machined by the Army Mechanics and Materials Research Center, Watertown, Massachusetts from Rockwell International material.

The chemical analyses of the alloys used in SCC tests are provided in Table 4. Oxygen, hydrogen and nitrogen analyses were not obtained. These elements are, however, present in the microstructure in the form of blocky carboxynitride inclusions and hydrogen, after exposure to the environment, in the form of very small lenticular uranium hydride inclusions near the surfaces.

The materials were fabricated into rectangular plate according to the thermomechanical processing schedules given in Table 5. Designations for the various treatments are also indicated in Table 5.

Some specimens of the U-2Mo QOA were reheat treated to form a two phase structure by quenching from the $\alpha+\gamma$ phase field. The resulting microstructure is shown in Figure 3(a). The morphology consists of a dispersion of retained γ, rich in molybdenum, imbedded in a low molybdenum α matrix. There is no optical evidence in the micrographs that the banded martensitic variant of the α phase, α_b', was formed during the quench. The prior γ ASTM grain size is 2 to 3. Large rectangular precipitates, which presumably are carboxynitrides, are also found in the fracture topology.

The quenched and overaged U-2Mo QOA microstructure is seen in Figure 3(b). It consists of small precipitates of δ along prior γ grain boundaries and psuedo-lamellar (α + δ) in the grain interior. The prior γ grain size is ASTM 2 to 3. Again, there are some small blocky carboxynitride inclusions dispersed throughout the microstructure.

In Figure 3(c), the microstructure for the uranium -3/4 Quint (U-3/4 Quint) is given. The structure is similar to the quenched and overaged U-2Mo. In this case, however, the ASTM grain size number is 3 to 4.

The microstructure of the as extruded uranium -3/4 w/o titanium (U-3/4 Ti) material is presented in Figure 3(d). The structure is the acicular form of martensitic α_a', and is very similar to what one would expect for a γ quenched and overaged material. The morphology shows some decomposition at the prior γ grain boundaries and inside the martensitic needles. Some inclusions are also observed. The prior γ average grain diameter is 300 μm.

The mechanical properties of these alloys are given in Table 6 at several humidity levels. Tensile and Charpy V-notch bars were machined from cantilever beam bars after SCC testing. The Poisson's ratio was assumed to be 0.22. Charpy data is shown in Figure 4.

II. RESIDUAL STRESS MEASUREMENTS

The most widely used mechanical method giving a three-dimensional evaluation of internal stresses in metals is the boring-out method proposed by Mesnager[7], developed by Sachs[8], and discussed widely in the literature[9]. Boring-out experiments were performed on rounds fabricated by grinding hot rolled rod, by forging, and by casting.

The experimental method consisted of boring out the center of a projectile in a succession of small layers and measuring the resultant

mechanical relaxations in the length and diameter of the remaining portion of the round after each bore. In the present experiments 120 Ω Magnaflux PA-09-062 AH-120 gages were used to measure relaxation strains. The gages were mounted to the cylindrical section of the rounds with either Eastman 910 cement or M-Bond 610 adhesive. Some difficulty was experienced in maintaining adherence of the gage because of oxidation of the alloy at the adhesion site. Short times between gage mounting and boring minimized this problem. Eastman 910 proved to be the better adhesive choice. The gages were coated with a silicon-phenolic resin to protect them from oil, water, and impact damage during handling.

Borings were performed with extreme care under a 40:1 mixture of water and water soluble oil. This was to prevent overheating with resultant annealing and to prevent introducing erroneous stresses during cutting of the metal. A photograph of the set-up without the coolant is shown in Figure 5.

Strain measurements were made after each bore when the relaxation was complete. A BLH model 120C strain gage power supply and bridge was used.

III. SCC TESTING

Stress corrosion testing was performed on the depleted uranium alloys to obtain crack growth kinetics. The test apparatus was a cantilever beam fixture similar to that proposed by Brown and Beachem[4]. Cantilever beam specimens were instrumented with a crack-opening-displacement gage to continuously monitor crack growth rate. A schematic of the test arrangement is shown in Figure 6. The system is capable of distinguishing crack opening displacement changes of 1×10^{-3} mm which gives a system resolution of 0.5 mm for a period of one month. Crack growth rates of 3.5×10^{-4} mm/hr can be detected in less than seven days.

Prior to testing, the specimens were fatigue precracked to insure a sharp notch. Crack orientation was TS. Fatigue precracking was performed in a cantilever configuration for the 12.7 mm x 12.7 mm x 152.4 mm samples on a constant deflection Krauss-Tatnal machine and in three point bending for the 25.4 mm x 25.4 mm x 152.4 mm samples on a closed-loop machine. The fatigue schedule was well within the criteria established in ASTM E399-74 with the ratio of the maximum stress intensity of the fatigue cycle, K_f (max) to the Young's modulus E, equal to 8.01×10^{-5} $m^{1/2}$ for the final 1.5% overall length of notch plus crack. The ratio of K_f(max) to K_{IC} was at most 0.3; and the plastic zone radius, using Irwin's approximation, at the beginning of the SCC test was 1.38×10^{-5} to 1.76×10^{-5} m.

The specimens were dipped in a 3.5 percent salt distilled water solution. The specimens were allowed to dry in laboratory air. The specimens were then installed in the cantilever beam test apparatus with zero applied load for one hour in a closed container designed to maintain 98 percent relative humidity. The solution in the container was a super-saturated solution of $CaSO_4.5H_2O$ in distilled water as specified by ASTM E104-51 (Reapproved 1971), located about 35 mm below the specimen. After the one hour necessary for the atmosphere to equilibrate around the specimen, the test load was applied. Room temperature and room relative humidity were continuously monitored. Additional details of this test procedure are given in reference 10.

RESULTS AND DISCUSSION

Illustrated examples of residual stress distributions for various rounds tested are shown in Figures 7 and 8. A generalized comparison of stress distribution versus fabrication technique shows the ground, hot rolled, material to have large tangential tensile stresses on the surface (of the order of 380 MPa) whereas forged and cast penetrators are either in a compressive surface stress state or exhibit considerably lower tensile surface stress (max 100 MPa).

The surface stress state is critical in determining susceptibility to stress corrosion cracking. A large tensile surface stress component coupled with flaws or inclusions results in SCC failures. The ground, hot rolled material #16 and #18 exhibit this type of stress distribution. "As forged" rounds 3808, 3811, and 3798, however, showed compressive stress states on the surface. This minimizes the likelihood of stress corrosion failures; and, indeed, no SCC failures have been observed in forged penetrators.

The cast rounds of lots 1 and 2 and the forged rounds of lots A and C show minimal stress. In comparison, the cast lot 4 sample which has been cast and remelted three times retained a higher stress level. Also, the "as forged" lot F and lot D rounds showed this trend. It was believed that heat treatment of the forged rounds might achieve some stress relief. The data indicates that this assumption is not correct for all heat treatments.

Another interesting result is that in many instances large hydrostatic tensile stresses were present along the centerline of the rounds. Although no centerline porosity was observed metallographically, the possibility of this occurring remains. Centerline porosity has been a problem in parts fabricated from U-3/4 Ti. Sachs boring out data for a 34.9 mm dia (1-3/8 in)

by 101.6 mm long (4 in) U-3/4 Ti bar water quenched from 800°C showed high centerline tensile stresses with σ_ℓ = 758 MPa (110 Ksi) and σ_t = 586 MPa (85 Ksi)[3]. The stresses decreased monotonically toward the outer surface and became compressive with σ_ℓ = -345 (-50 Ksi) and σ_t = -552 (-80 Ksi). Results on a 25.4 mm dia (1 in) rod are reported to be similar. Northcutt reports fabrication procedures which prevent centerline void formation in DU-3/4 Ti long rod penetrators.[11]

Stress corrosion cracking (SCC) is a fracture process caused by the conjoint action of stress and corrosive environment. Surface tensile stresses are necessary for SCC. To quantify safe operating stresses it is common practice to use the concepts of linear elastic fracture mechanics. This approach assumes that the propagation of cracks is predictable in terms of the magnitude of the tensile stresses at the crack tip and that the opening of the crack is controlled by the stress intensity factor, K. The K level which causes fast fracture solely because of overload is designated K_{IC}. The threshold (if it truly exists) above which SCC occurs is designated K_{ISCC}. Figure 9 schematically shows expected da/dt vs. K_I data with three stages, I, II, and III of kinetic behavior.

Typical normalized crack length-time curves are shown in Figure 10. Although at first glance the curves appear relatively smooth, they contain fine details which suggests that "crack propagation is irregular." First, many samples exhibited a rapid increase in crack length during the early part of the test as illustrated by curve A. This produces an initially decreasing crack growth rate, da/dt, with increasing K_I as shown in Figure 11 for a DU-3/4 Ti alloy. This behavior is possibly caused by crack tip blunting due to corrosion and/or residual stresses. Secondly, cracks frequently increased their crack lengths with rapid jumps in length over relatively short periods of time as indicated by curve B of Figure 10. This behavior

causes fluctuating da/dt with increasing K_I and occurs in both large and small steps as shown in Figure 12 for a DU-2Mo QOA material. The DU-2Mo ($\alpha + \gamma$) and DU-3/4 Quint materials behaved similarly. This behavior could also be due to residual stresses or corrosion product wedging.

All alloys showed stage II and III crack growth behavior. Stage I crack growth kinetics were not observed even though growth rates as low as 10^{-9} m/sec were measured. This contrasts with the work of Magnani[12] on a DU-4.5 w/o Nb alloy which showed a distinct stage I in low humidity air at a comparable sensitivity.

Initial stress intensity, K_I, as a function of time-to-failure (TTF) is shown in Figure 13. For SCC resistance in salt laden moist air, the alloys rank in the order DU-3/4 Ti, DU-2Mo QOA, DU-2Mo ($\alpha + \gamma$), and DU-3/4 Quint. Threshold values, K_{ISCC}, are listed in Table 7 and ranged from 24.2 MPa$\cdot$m$^{1/2}$ to 15.6 MPa$\cdot$m$^{1/2}$. K_{ISCC} values for the DU-2Mo alloys were not significantly lower than the value for DU-3/4 Ti. Fracture toughness decrease because of exposure to the environment, however, was much more significant for the DU-3/4 Ti and DU-3/4 Quint alloys than it was for DU-2Mo.

Interpretation of SCC fracture surfaces examined by SEM was difficult because corrosion obscured many fracture features. Some general fracture trends were, however, evident. Typical fracture surfaces for U-2Mo are shown in Figure 14(a)-(c). Figure 14(a) shows the fracture surface of U-2Mo QOA near the boundary of the transition of slow crack growth to fast crack growth. The fracture morphology is predominantly mixed intergranular and quasicleavage with separation at $\alpha + \delta$ lamella a frequent observation. This fracture morphology at higher K values, Figure 14(b), does not contain intergranular fracture but appears to show mixed quasicleavage and ductile dimple tearing. Figure 14(c) shows the morphology of the U-2Mo ($\alpha + \gamma$) at high K. It, too, consists of quasicleavage and dimples; however, there is

a much larger fraction of ductile fracture and the involvement of the large blocky precipitates in the fracture is evident. These observations are in agreement with those of Fishman and DeJarnette[13], but differ somewhat from the observations by Koger and Bennett[14] on higher Mo content alloys. The latter authors observe a preponderance of intergranular fracture in aqueous chloride environments.

Fracture surfaces for U-3/4 Ti were more uniform in appearance as K increased. Typical fractures are shown in Figure 15(a) and (b). In Figure 15(a), separation at α' platelets is apparent and the fracture appears ductile between platelets, although definite dimple morphology was not observed. A higher magnification view, shown in Figure 15(b), shows some quasicleavage with secondary cracking apparent. A cross-sectional micrograph is shown in Figure 15(c) which shows only a slight, but definite, tendency to cleave α' platelets.

Stress corrosion cracking fracture morphology of U-3/4 Quint is shown in Figure 16(a) through (c). The region of slow crack growth was flat and transgranular with some ductile appearance as shown in Figure 16(a). At higher K values a transition in fracture mode to intergranular separation along prior γ grain boundaries occurs. The intergranular separation is not smooth as would be expected with grain boundary decohesion, but consisted of mixed quasicleavage in ill-defined river patterns connected by distorted regions as shown in Figure 16(c).

CONCLUSIONS

The principal results of this investigation and the conclusions drawn from them are as follows:

1. Depending on manufacturing method, residual surface stresses may be either tensile or compressive. Tensile stresses should be avoided since

they aggravate SCC. Hot rolled and ground rounds showed the highest level of residual surface tensile stresses which were often above the SCC threshold, σ_{SCC}, in magnitude. Forged and heat treated rounds and cast rounds also showed tensile residual stresses on the surface. These stresses, however, were lower in magnitude and below σ_{SCC}.

2. Direct correlation of SCC behavior between residual stress level, measured K_{ISCC} values, and the moist nitrogen test was obtained.

3. Large hydrostatic tensile stresses were observed along the centerline of some rounds, thus, introducing the possibility of centerline void formation. Centerline void formation was not, however, observed.

4. There is little difference in SCC resistance between U-3/4 Ti, U-2Mo, and U-3/4 Quint alloys in salt laden moist air environments. U-3/4 Ti and U-2Mo show a slightly higher resistance than does U-3/4 Quint.

5. U-3/4 Ti and U-3/4 Quint show a much larger decrease of toughness when exposed to the environment than does U-2Mo.

6. Stage I crack growth kinetics were not observed in these alloys at crack velocities as low as 10^{-9} m/sec.

7. Continuous monitoring of crack growth rate revealed that crack propagation is not continuous.

REFERENCES

1. S. G. Fishman and C. R. Crowe, Pract. Metallog., 13, 184 (1976).

2. S. G. Fishman and C. R. Crowe, in Case Studies in Fracture Mechanics (AMMRC; Watertown, MA:1977) MS 77-5.

3. A. M. Ammons, in Physical Metallurgy of Uranium Alloys, J. J. Burke, et. al., ed. (Brook Hill: Chestnut Hill, MA: 1976) p525.

4. B. F. Brown and C. D. Beachem, Corr. Sci., 5, 745 (1965).

5. B. F. Brown, Stress Corrosion Cracking in High Strength Steels, and in Titanium and Aluminum Alloys, (Naval Research Laboratory, Wash.,D.C.,1972)1.

6. J. G. Kaufman, Marshall Space Flight Center Rept., No. NAS-8-21484, May 31, 1973.

7. M. Mesnager, Comptes Rendus, 169, 1391 (1919).

8. G. Sachs, Z. Metallkunde, 19, 29 (1929).

9. J. J. Lynch, in Residual Stress Measurements, R. G. Trenting, et.al., eds. (ASM: Metals Park, Ohio: 1952)51.

10. J. A. Joyce, D. F. Hasson, and C. R. Crowe, J. T. E. V. A., 8, 293 (1980).

11. W. G. Northcutt, Union Carbide Corp., Oak Ridge Y-12 Report Y-2128,1978.

12. N. J. Magnani, in Advances in Corrosion Science and Technology, 6, M. G. Fontana and R. W. Staehle, eds., (Plenum: New York: 1976) 89.

13. S. G. Fishman and H. DeJarnette, Corr., 33, 351 (1977).

14. J. W. Koger and R. K. Bennett, Union Carbide Oak Ridge Y-12 Plant Report No. Y-2063, 1976.

LIST OF FIGURES

Table 1

Manufacturing Detail for Rounds

Tested for Internal Stress Distribution

Round Identification	Manufacturer	Method Used to Produce Rounds
16', 18'	NL Industries	Hot rolled then machine ground
3798'	NETCO	Solution treated @ 850°C, 40 min. OQ → aged 582°C, 8 hrs, then forged 2 blows @ 500°C
3808'	NETCO	As Forged @ 620°C, 1 blow
3811'	NETCO	As Forged @ 500°C
Lot A #4	NETCO	Forged @ 500°C heat treated 575°C, 1 hr R_c 28/32
Lot B #2	NETCO	Same as Lot A
Lot C #5	NETCO	Forged @ 500°C heat treated 525°C, 1 hr R_c 33/34
Lot D #3	NETCO	Forged @500°C, heat treated 450°C, 1 hr R_c 34/35
Lot F #1 #2	NETCO	Forged @ 500°C
Cast Lot I #6	NMI	Cast → solution heat treated @ 850°C, 40 min, OQ → aged @ 582°C, 8 hrs 340/460 ppmC
Cast Lot II #8	NMI	230/470 ppmC recycled
Cast Lot IV #7	NMI	930-960 ppmC recycled

Table 2

Chemical Analysis of the Depleted Uranium Rounds

	FORGED					CAST		
	A (ppm)	B (ppm)	C (ppm)	D (ppm)	F (ppm)	I (ppm)	II (ppm)	IV (ppm)
Aluminum	50	70	60	50	100	30	70	70
Copper	10	10	10	10	200	70	70	30
Iron	15	15	15	15	40	20	20	20
Magnesium	7	5	7	7	30	5	10	10
Manganese	15	7	5	5	10	20	30	20
Nickel	40	40	20	20	70	150	150	70
Lead	15	15	10	10	30	5	5	2
Silicon	300	250	10	10	30	400	700	700
Cobalt	20	20	20	15	20	20	20	20
Zirconium	10	10	10	10	10	10	10	10
Oxygen	520	800	550	190	130	250	200	140
Hydrogen	4	2	2	2	3	2	1	1
Nitrogen	30	30	30	40	40	30	20	40
Carbon	235	280	220	160	215	300	530	1000
Molybdenum (wt pct)	1.89	1.88	2.11	2.20	1.98	1.98	2.10	1.89
U remains	97.98	97.96	97.79	97.75	97.93	97.89	97.72	97.90

Data taken by Ledoux and Co., Teaneck, NJ

Table 3

Hardness and Strength Data

Lot	Hardness (Rock. C) ± 2	Yield Strength MPa(Ksi)
A	29	658.4(95.5)
B	28	No Data
C	33	742.5(107.7)
D	34	823.2(119.4)
F	31	637.7(92.5)
I	32	715.0(103.7)
II	32	657.7(95.4)
IV	31	740.5(107.4)

Table 4 - Chemical Analyses in Weight Percent for Depleted Uranium Alloys used in SCC Tests

	Alloy		
	U-2Mo	U-3/4 Ti	U-QUINT
Mo	2.00	96×10^{-4}	0.84
Nb	—	$<10 \times 10^{-4}$	0.70
Zr	—	—	0.86
Ti	$<1 \times 10^{-4}$	0.71	0.44
V	$<1 \times 10^{-4}$	$<1 \times 10^{-4}$	0.16
Al	25×10^{-4}	35×10^{-4}	75×10^{-4}
Si	5.5×10^{-4}	127×10^{-4}	97×10^{-4}
Fe	60×10^{-4}	45×10^{-4}	140×10^{-4}
Cu	10×10^{-4}	10×10^{-4}	15×10^{-4}
C	100×10^{-4}	10×10^{-4}	40×10^{-4}
U	Balance	Balance	Balance

Table 5 - Thermomechanical Processing of Depleted Uranium Alloys used in SCC Testing

Alloy	Processing
U-2Mo QOA	γ extruded into rectangular plate at 100°C, solution treated for 2 hours and helium quenched; and aged at 500°C for 5 hours and air cooled.
U-2Mo (α+ γ)	As per U-2Mo QOA above plus: solution treat at 800°C for two hours, and water quenched: heated to 615° for five hours and water quenched: aged at 400°C for five hours, and slow cooled.
U-3/4 Quint	As extruded at 1000°C
U-3/4 Ti	As α extruded at 630°C

Table 6 - Mechanical Properties of Depleted Uranium Alloys In Dry Air and Salt Laden Moist Air

Material	%RH	0.2% Y.S. (MPa)	UTS (MPa)	%e (4D)	*** Rc	E(GPa)
U-2Mo QOA	0	796	1243	6.7	37.0	159
	98	735	1043*	-**		
U-2Mo (α+ γ)	0	642	952	3.0	37.0	164
	98	735	1126*	-**		
U-3/4 QUINT	0	721	1305	11.9	37.0	160
	66	728	1016*	1.5		
	98	742	1058*	1.6		
U-3/4 Ti	0	824	1339	7.1	37.0	172
	66	823	1036*	1.4		
	98	762	920*	1.5		

* Max Stress at fracture
** Specimen failed at artificial notch
*** Avg. of 5 readings

Table 7 - Comparison of Fracture Toughness and Threshold Stress Intensity for Depleted Uranium Alloys in 98% Relative Humidity Salt Laden Moist Air

Alloy	K_{IC} (MPa·$m^{1/2}$)	K_{ISCC} (MPa·$m^{1/2}$)
U-2Mo QOA	48.6	20.8
U-2Mo (α+ γ)	27.9	21.5
U-3/4 Quint	43.3	15.6

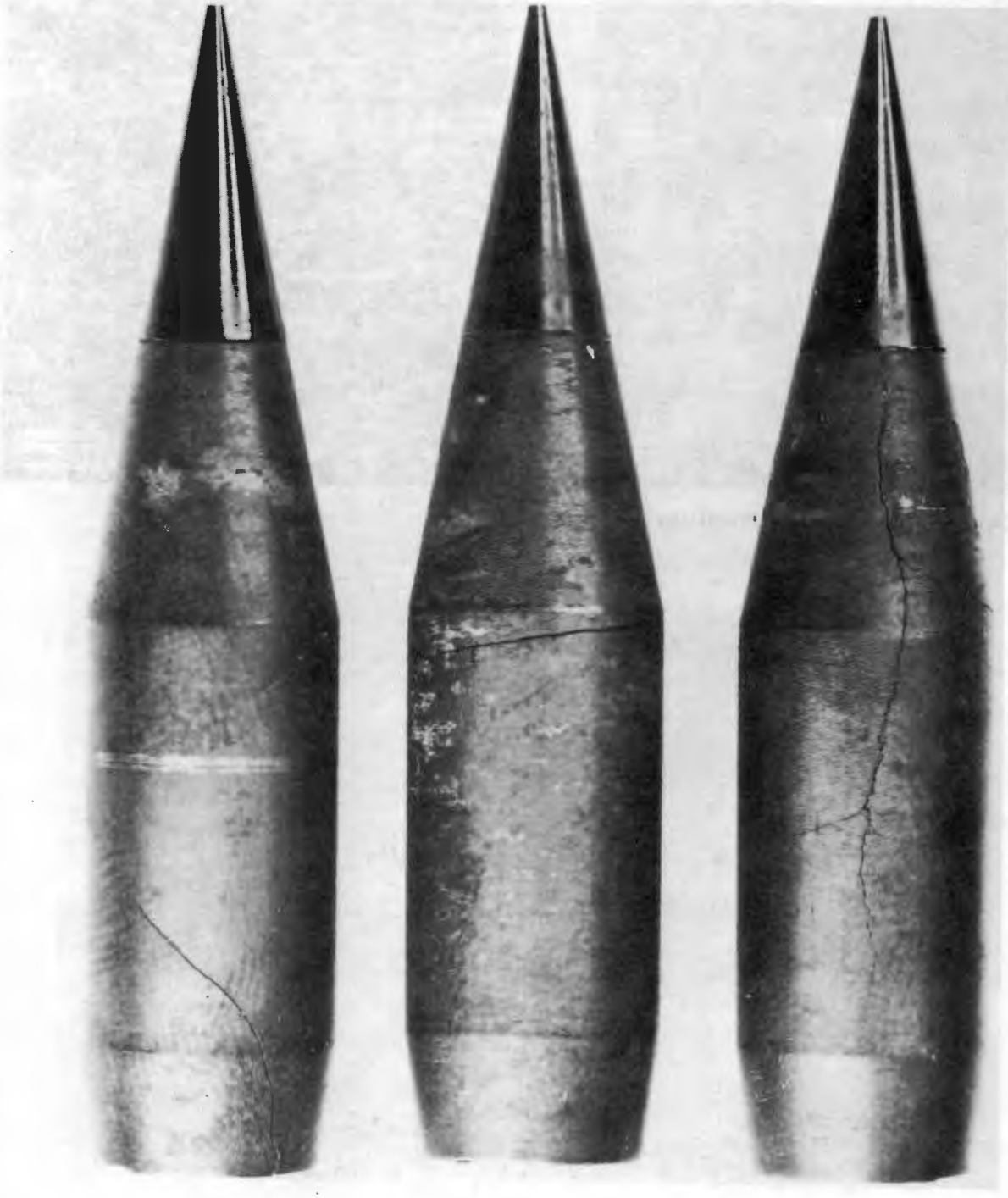

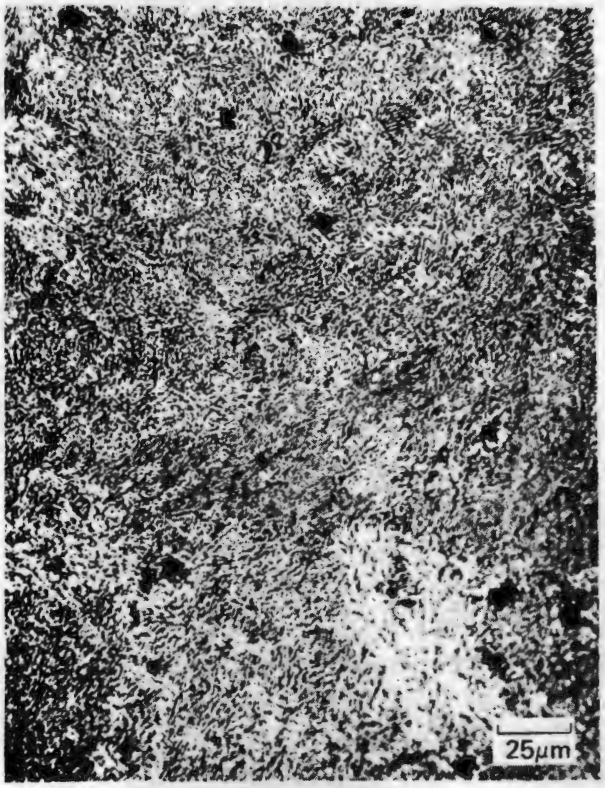

(A) HOT ROLLED AND GROUND

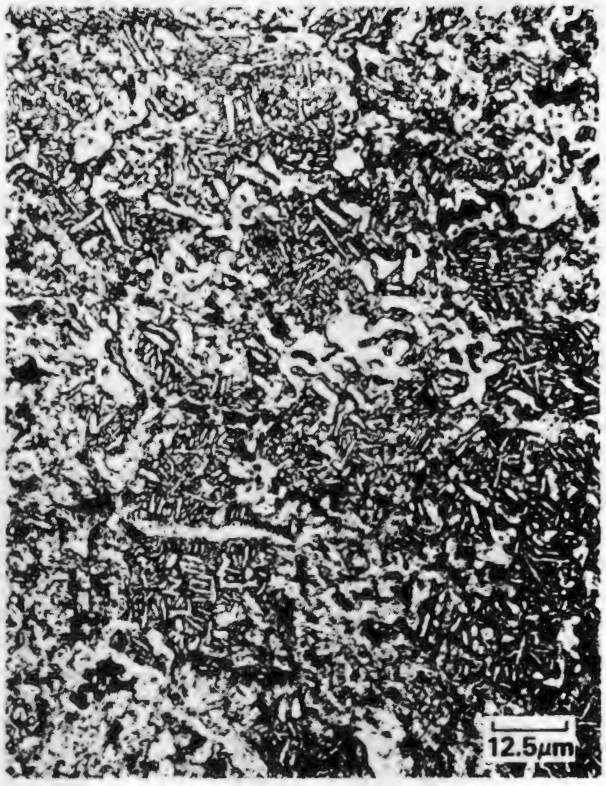

(B) FORGED

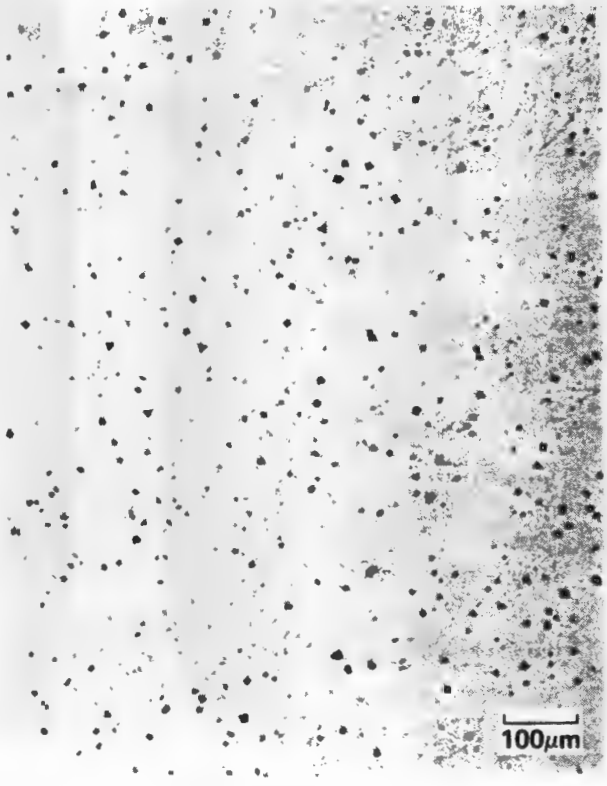

(C) CAST

FIGURE 2 INCLUSIONS OBSERVED IN PENETRATORS

(a)

(b)

(c)

(d)

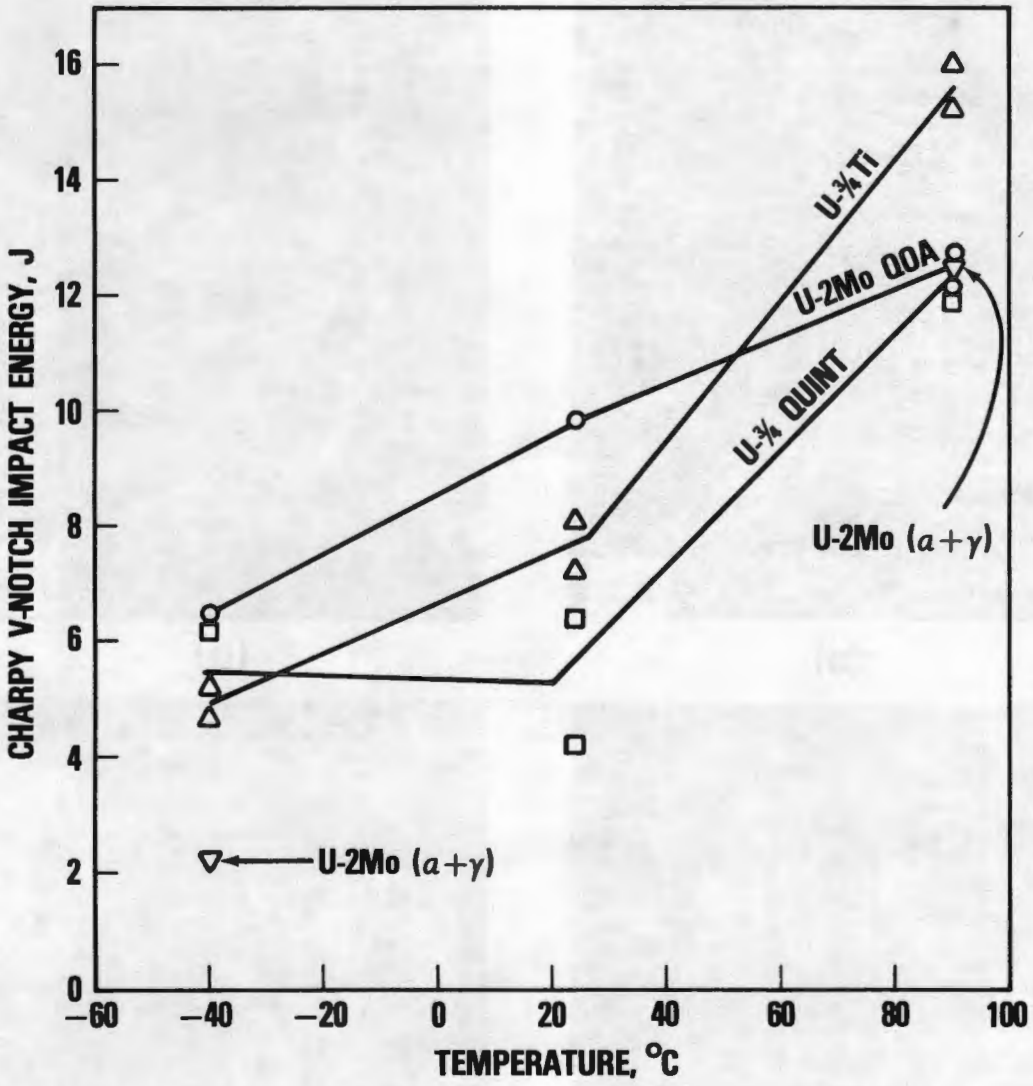
CHARPY V-NOTCH IMPACT ENERGY, J
TEMPERATURE, °C
U-¾Ti
U-2Mo QOA
U-¾ QUINT
U-2Mo (a+γ)
U-2Mo (a+γ)
0
2
4
6
8
10
12
14
16
−60
−40
−20
0
20
40
60
80
100

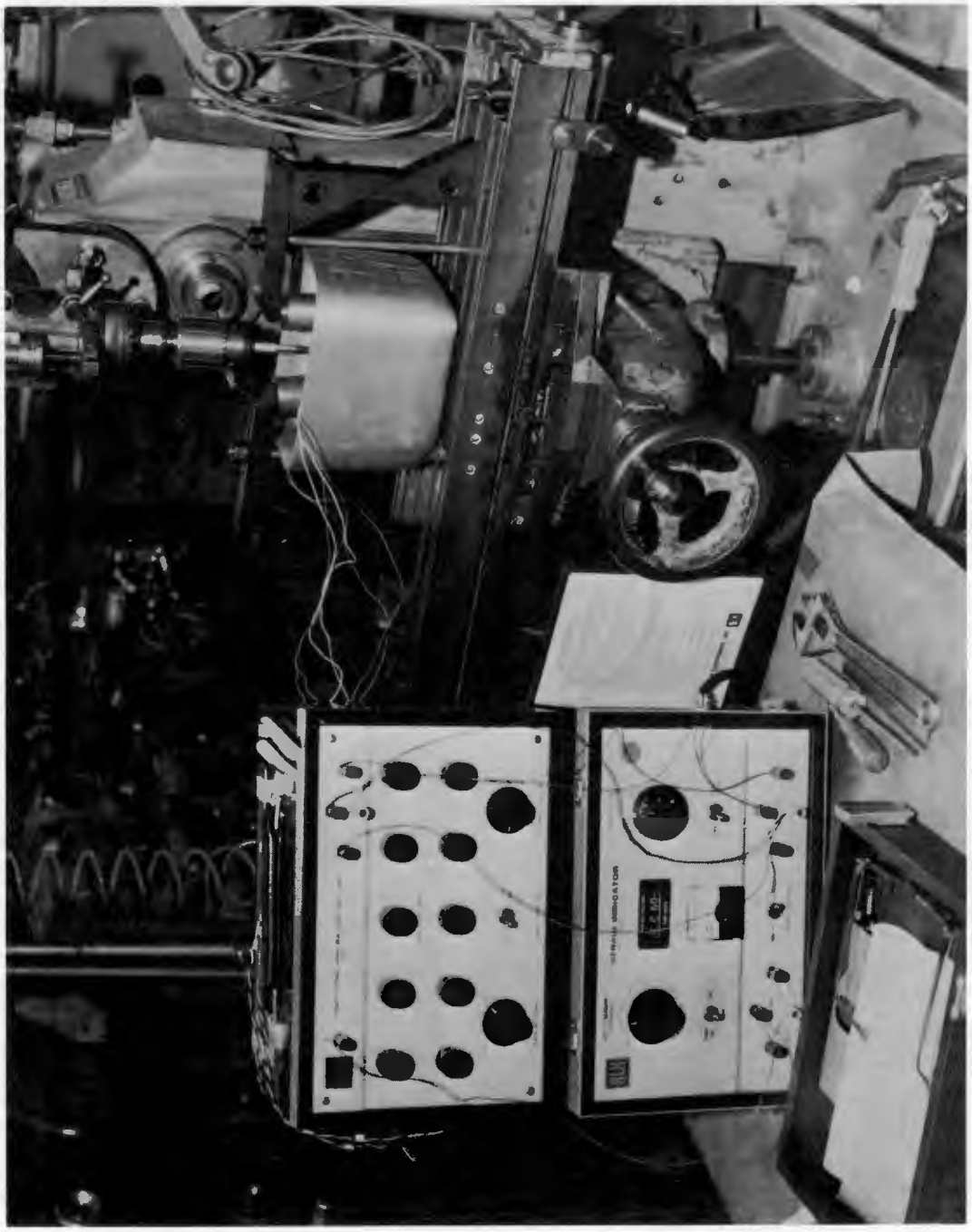

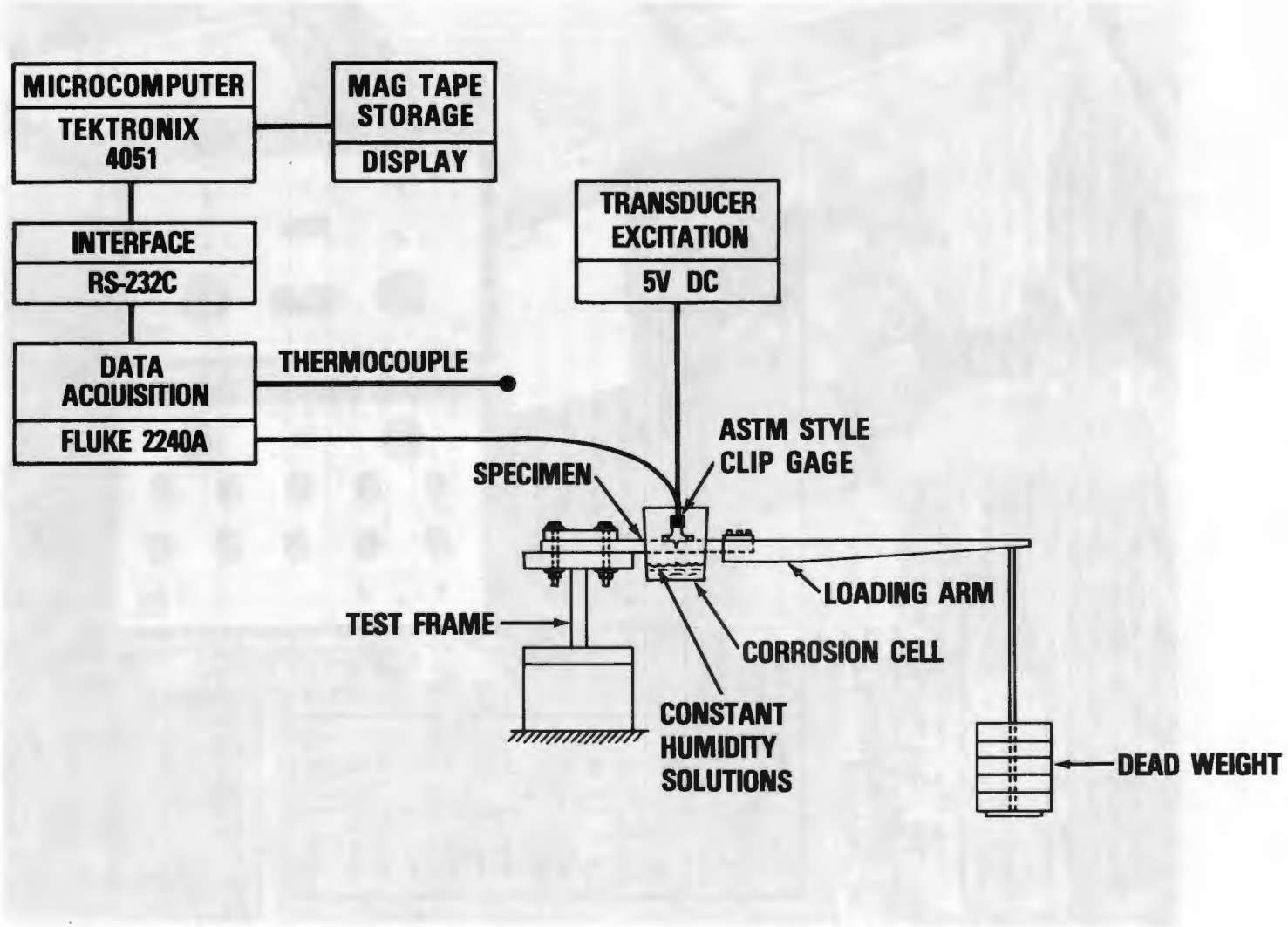
MICROCOMPUTER
TEKTRONIX 4051
MAG TAPE STORAGE
DISPLAY
INTERFACE
RS-232C
DATA ACQUISITION
FLUKE 2240A
THERMOCOUPLE
TRANSDUCER EXCITATION
5V DC
ASTM STYLE CLIP GAGE
SPECIMEN
LOADING ARM
TEST FRAME
CORROSION CELL
CONSTANT HUMIDITY SOLUTIONS
DEAD WEIGHT

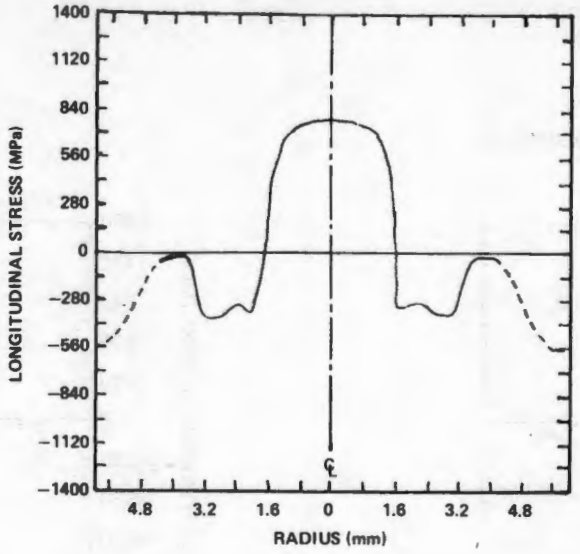
LONGITUDINAL STRESS (MPa)
1400
1120
840
560
280
0
-280
-560
-840
-1120
-1400
4.8
3.2
1.6
0
1.6
3.2
4.8
RADIUS (mm)

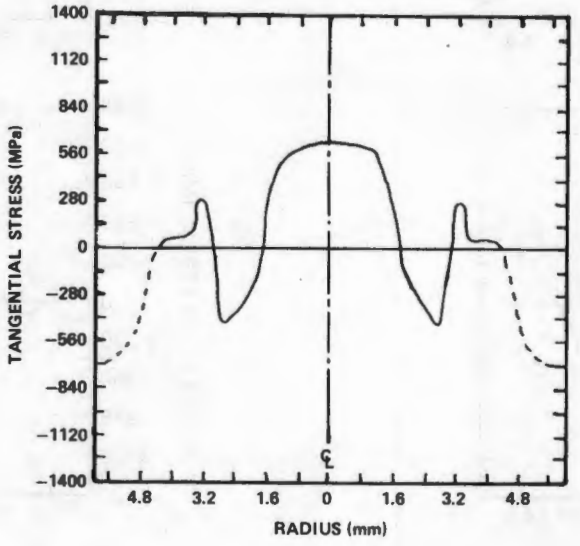
TANGENTIAL STRESS (MPa)
1400
1120
840
560
280
0
-280
-560
-840
-1120
-1400
4.8
3.2
1.6
0
1.6
3.2
4.8
RADIUS (mm)

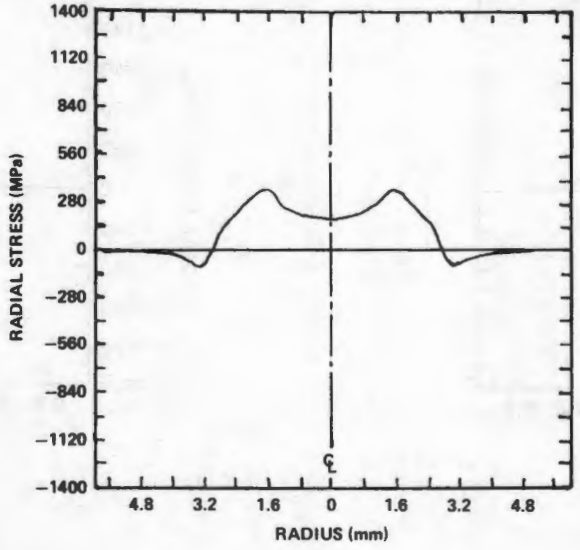
RADIAL STRESS (MPa)
1400
1120
840
560
280
0
-280
-560
-840
-1120
-1400
4.8
3.2
1.6
0
1.6
3.2
4.8
RADIUS (mm)

(A) HOT ROLLED AND GROUND #16

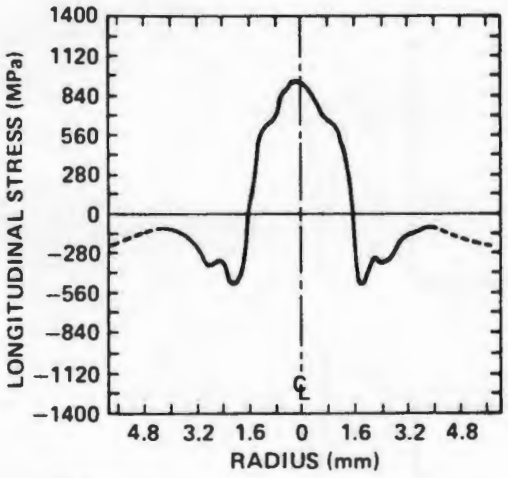

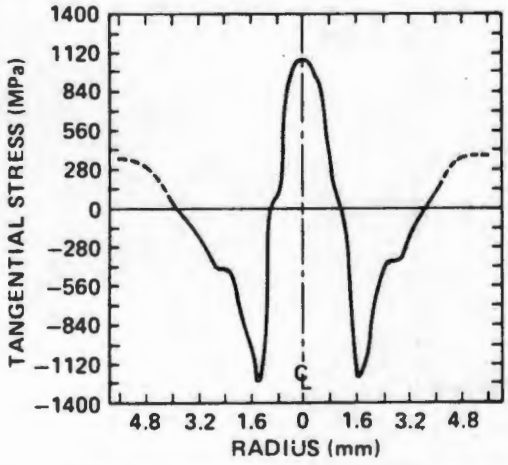

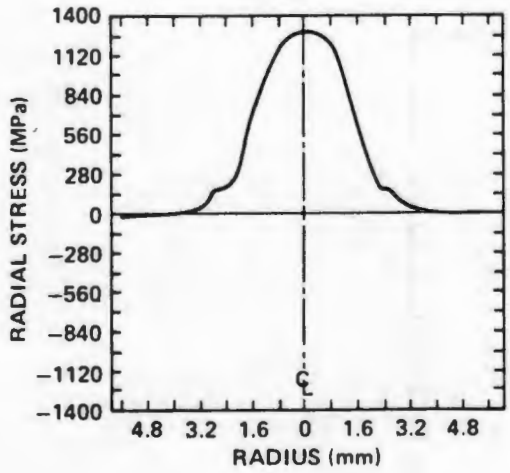

(B) CAST LOT #1

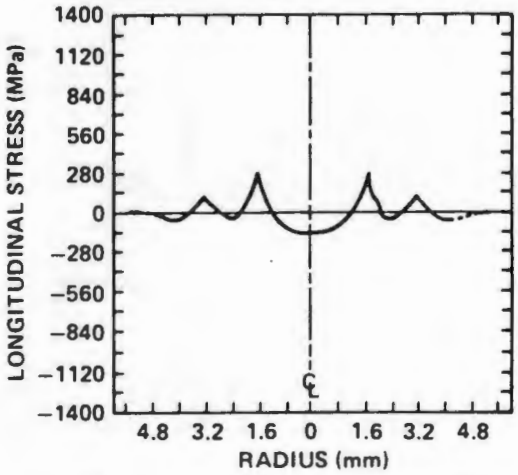

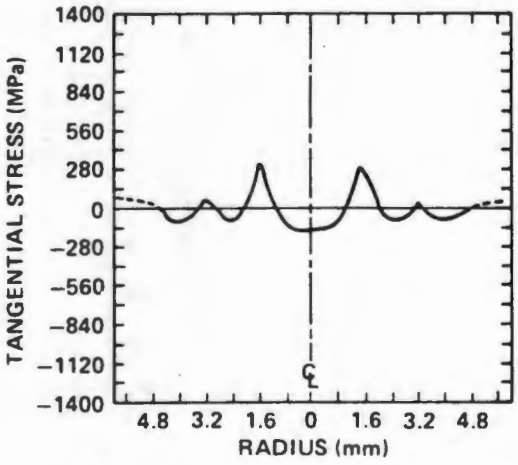

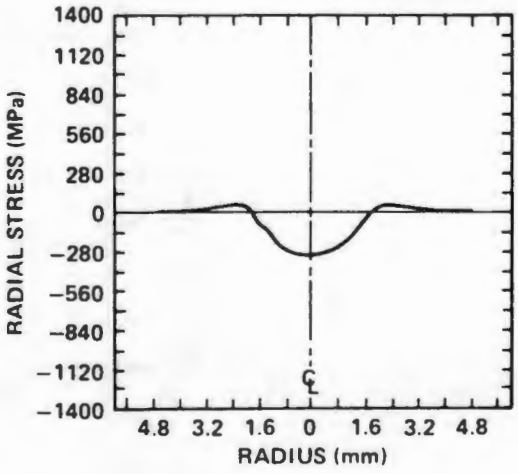

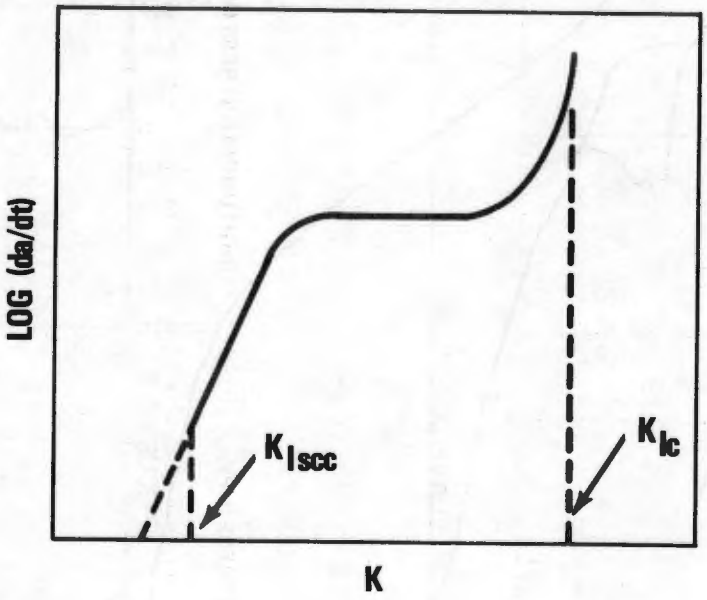
LOG (da/dt)
K_{Iscc}
K_{Ic}
K

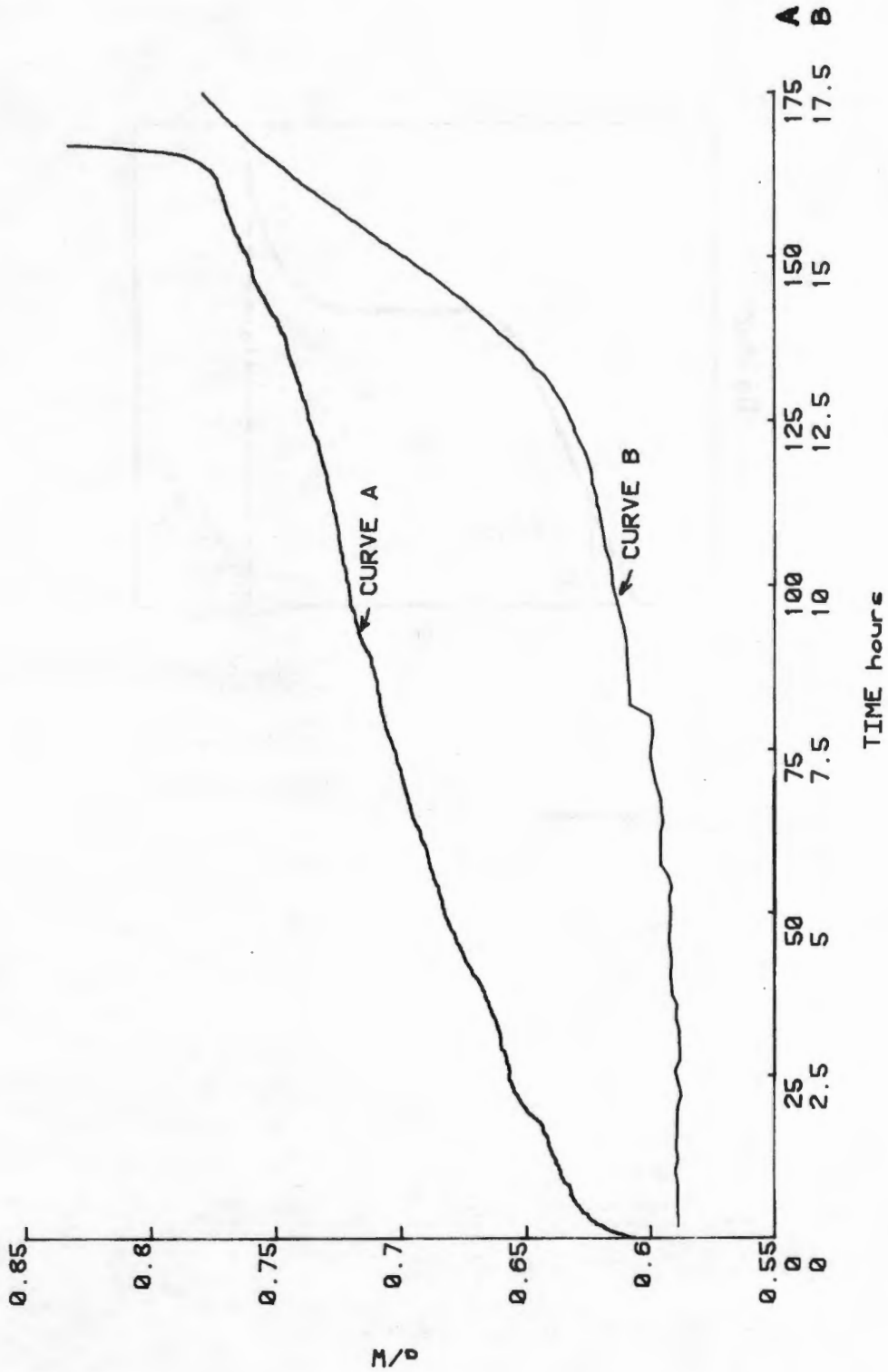
M/o
0.85
0.8
0.75
0.7
0.65
0.6
0.55
0
0
25
2.5
50
5
75
7.5
100
10
125
12.5
150
15
175
17.5
A
B
TIME hours
CURVE A
CURVE B

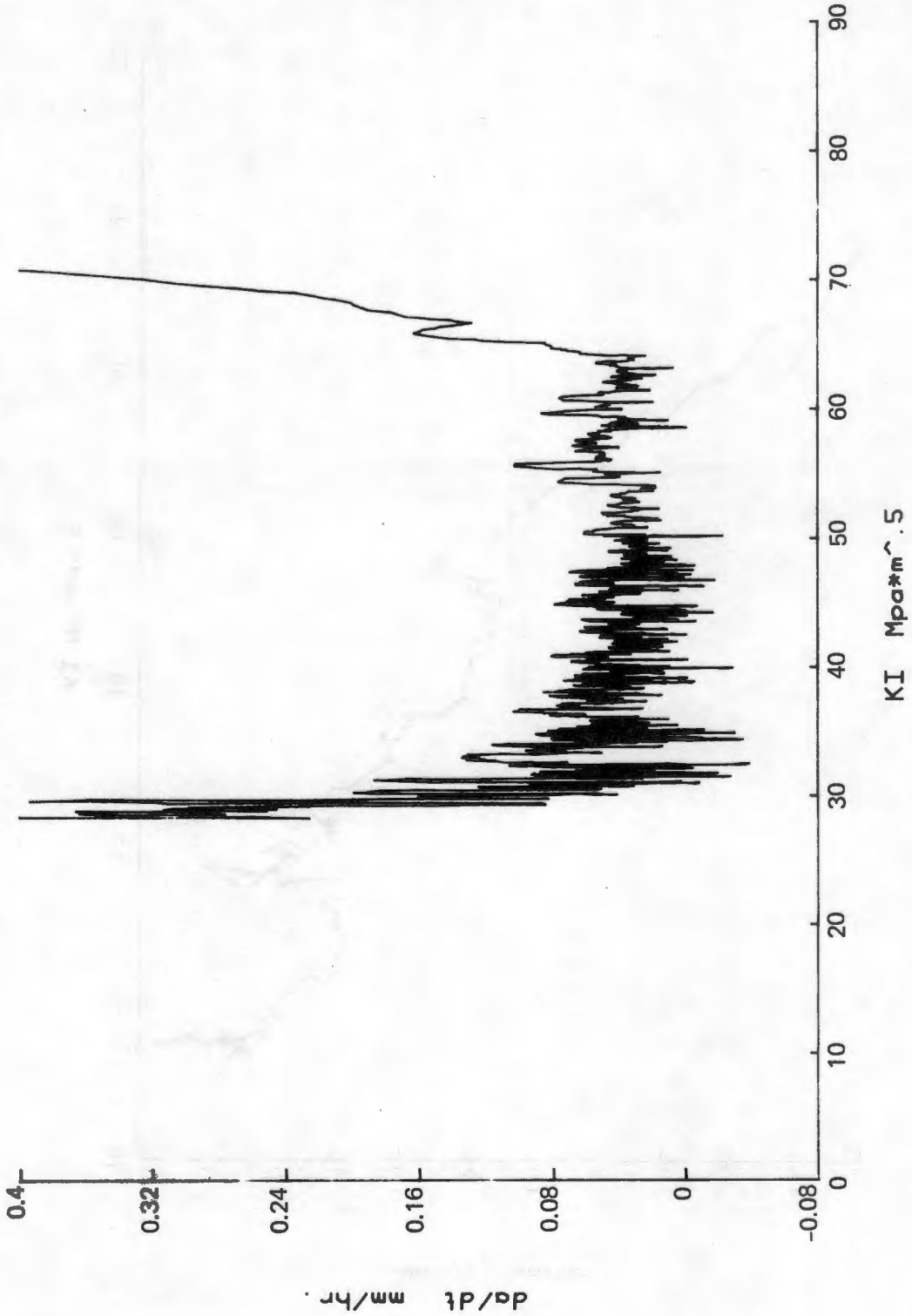
0.4
0.32
0.24
0.16
0.08
0
-0.08
da/dt mm/hr.
0
10
20
30
40
50
60
70
80
90
KI Mpa*m^.5

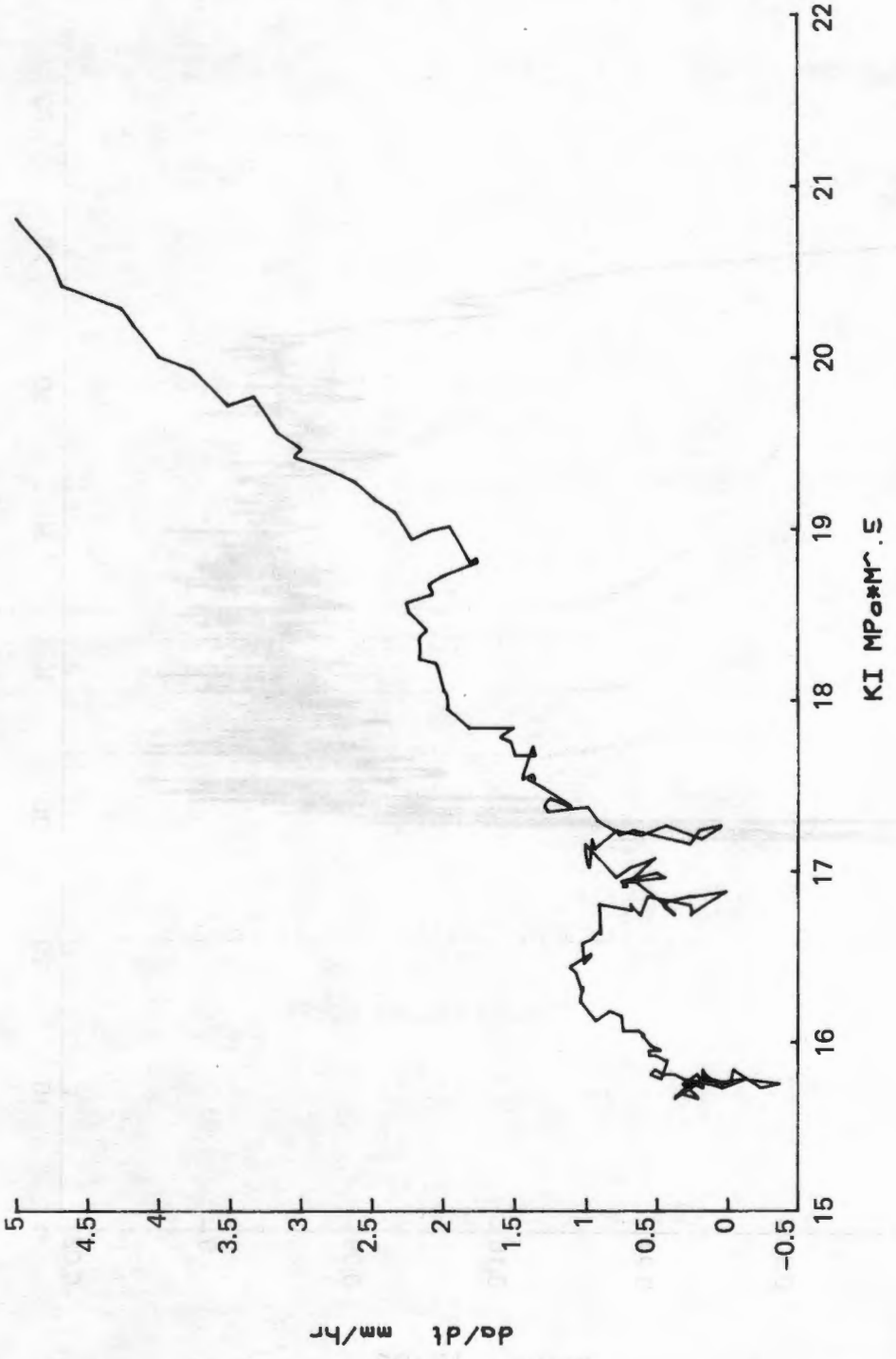
da/dt mm/hr
5
4.5
4
3.5
3
2.5
2
1.5
1
0.5
0
-0.5
15
16
17
18
19
20
21
22
KI MPa*M^.5

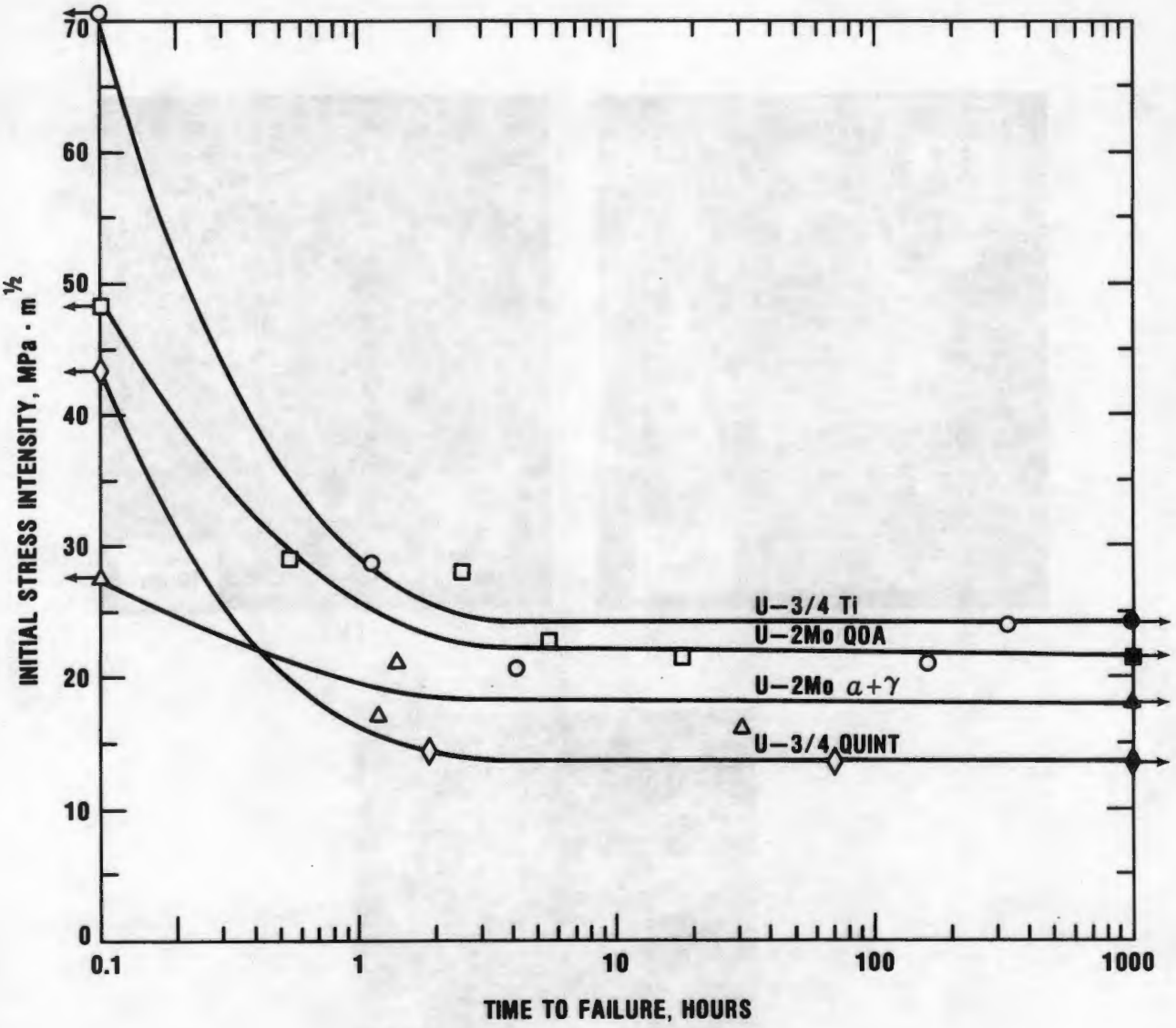
INITIAL STRESS INTENSITY, MPa · m^½
70
60
50
40
30
20
10
0
0.1
1
10
100
1000
TIME TO FAILURE, HOURS
U–3/4 Ti
U–2Mo QOA
U–2Mo α+γ
U–3/4 QUINT

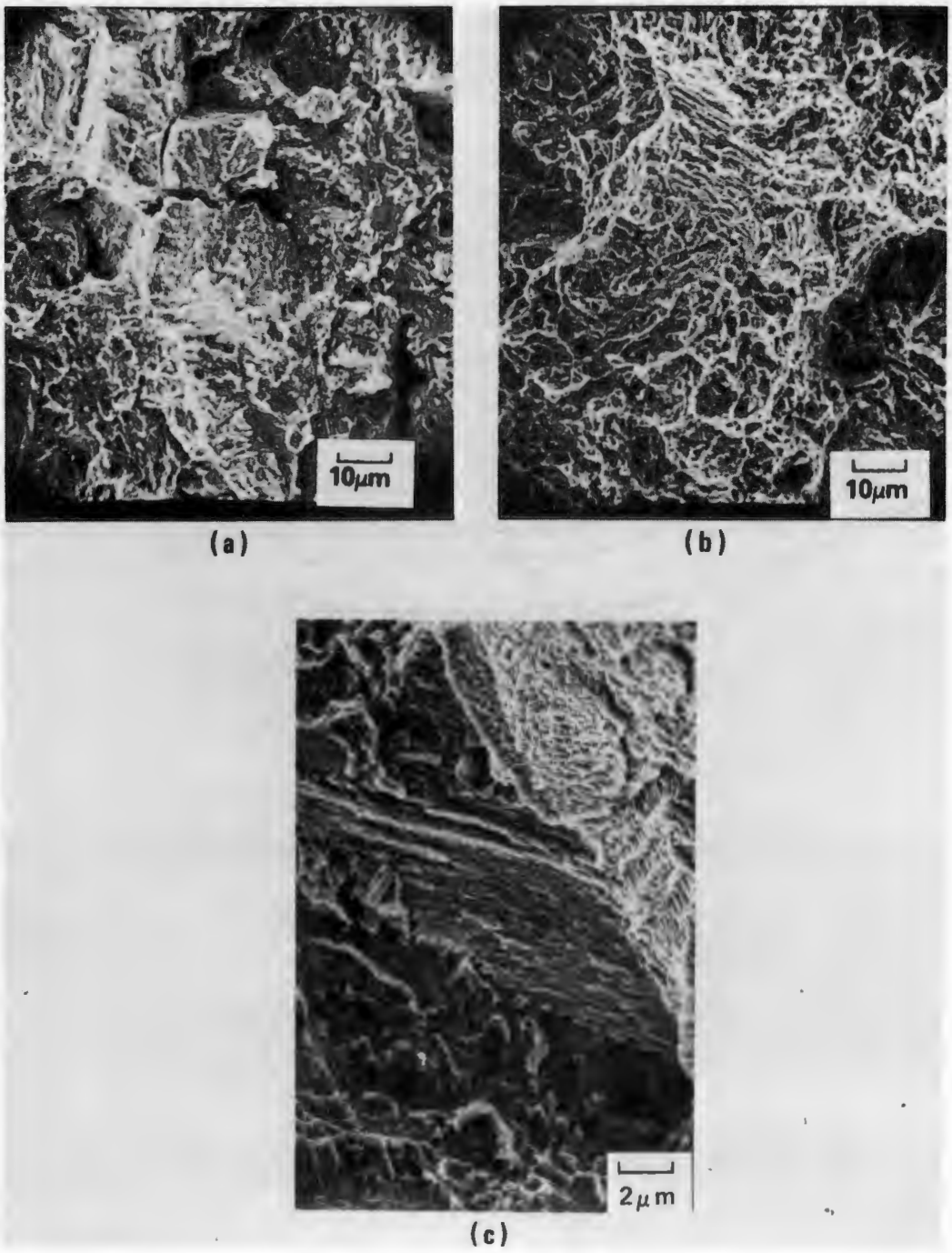
10μm
(a)
10μm
(b)
2μm
(c)

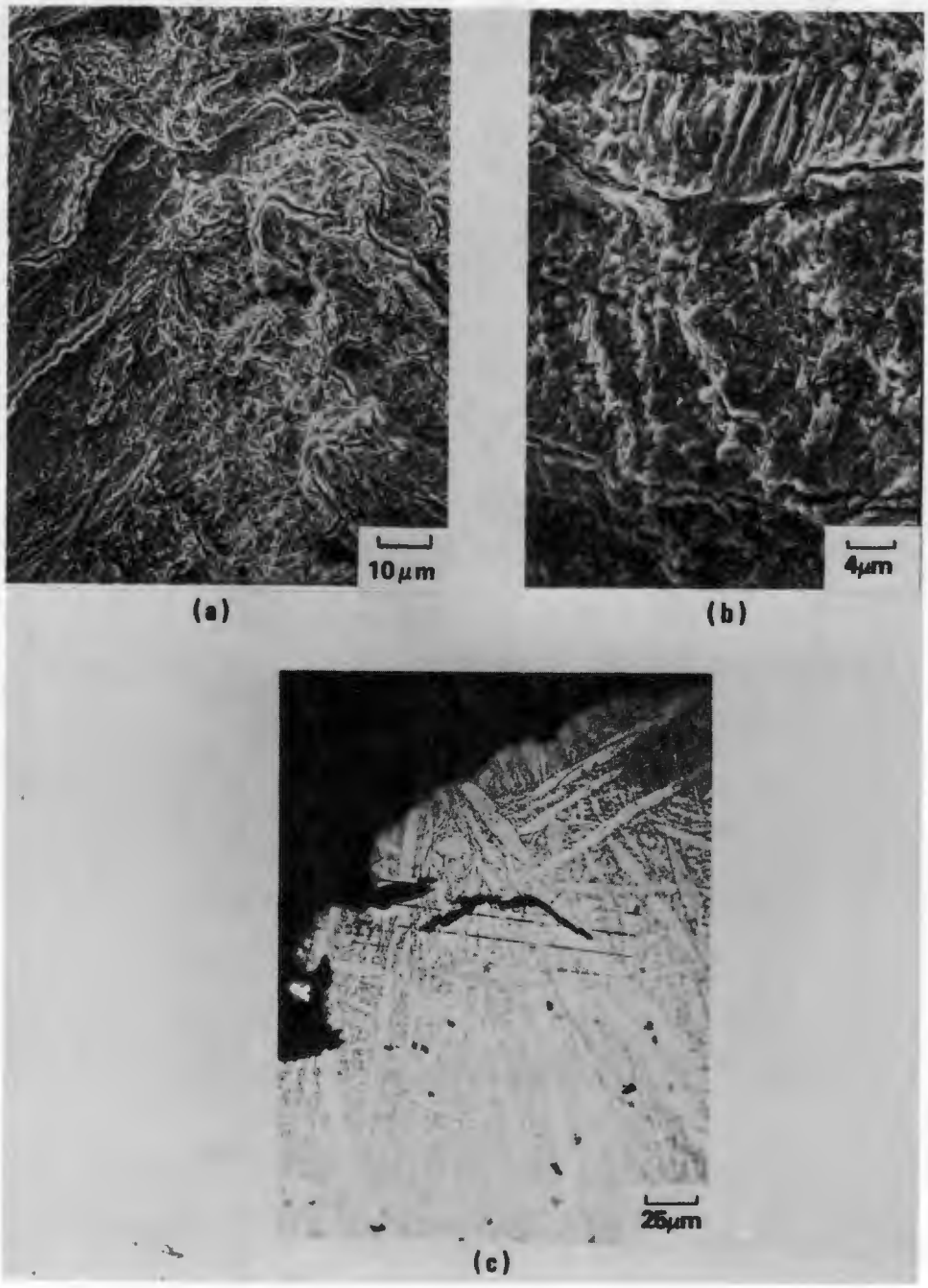
10μm
(a)
4μm
(b)
25μm
(c)

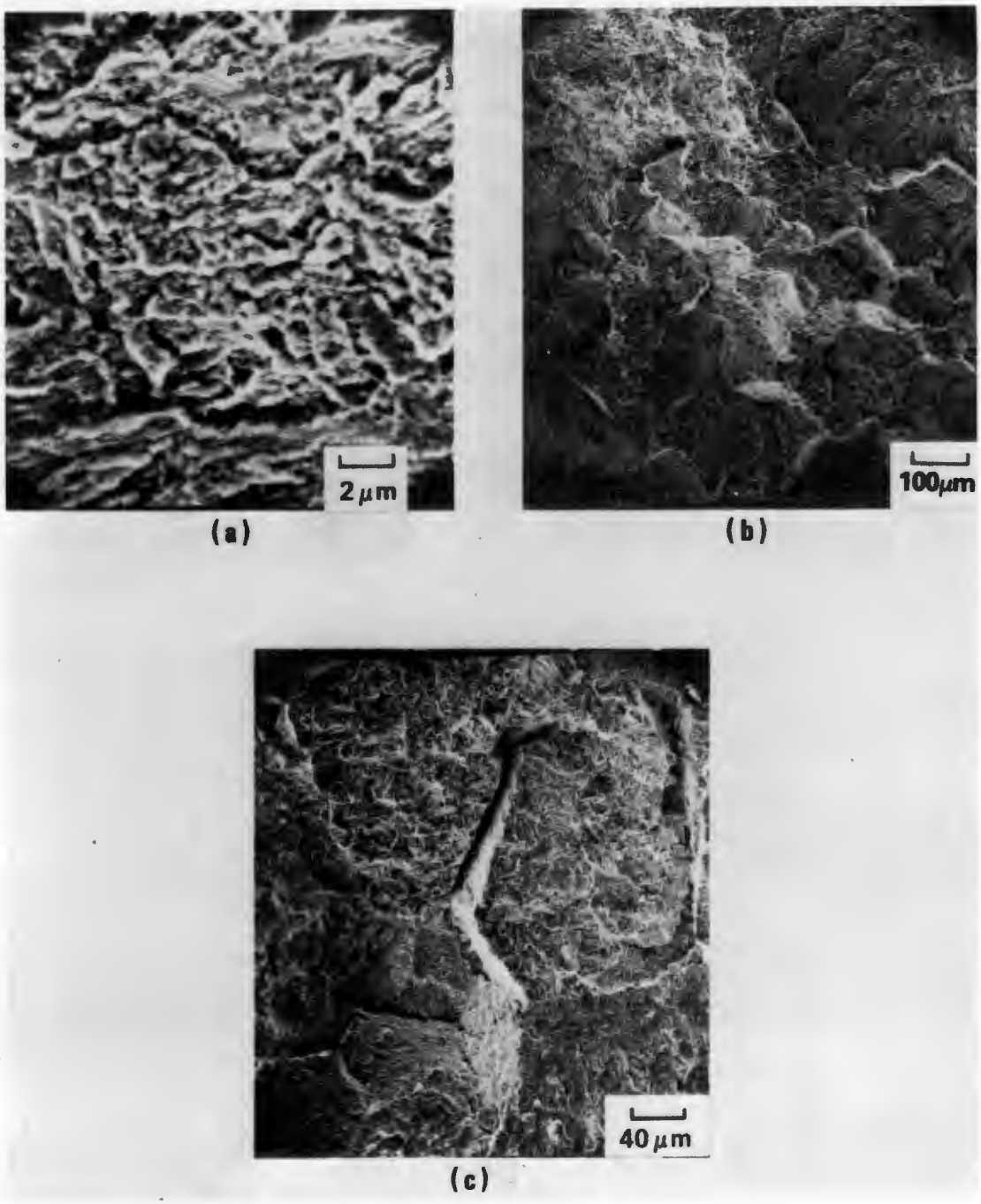
2 μm
(a)
100μm
(b)
40 μm
(c)